# 2.
# WATER-LOADED CONVENTIONAL METAL DIAGONAL HORN TERMINATED IN BIO-MEDIUM/BIO-MEDIA

## 2.1 Introduction

Conventional metal diagonal horn (MDH) is an unusual form of electromagnetic horn antenna having very peculiar property and it was first used by Tingye Li [Li (1959)] as a feed for illuminating the paraxial region of a spherical reflecting surface [Love (1976)]. In conventional MDH, standard rectangular waveguide carrying $TE_{10}$ mode is gradually transformed to circular waveguide carrying the $TE_{11}$ mode. Another gradual transition converts the circular cross sections into square, and the horn then flares out to the desired aperture size. All the cross-sections of the diagonal horn are square including the aperture. For small flare angles, the mode of propagation within the horn is principally such that the electric vector is parallel to one of the diagonals, when the electric field is excited diagonally, and hence it is referred to as diagonal horn.

The conventional MDH antenna terminated in free space which has attractive radiation properties was thoroughly investigated by Love [Love (1976)]. MDH has reasonable gain as well as beamwidth, and its radiation pattern in the far field possesses almost perfect circular symmetry so that the 3, 10 and 20 dB beamwidths are very closely equal, not only in the principal E and H planes, but also in the $45^o$ and $135^o$ planes [Love (1976)]. The wave which propagates in the slowly flaring MDH is composed of two equal amplitude and equi-phase conventional modes appropriate to square waveguide. One is a $TE_{01}$ mode; the other is its orthogonal counterpart, a $TE_{10}$ mode. Thus, the conventional MDH is a type of multimode horn in which the internal field consists of superposition of the orthogonal $TE_{01}$ and $TE_{10}$ modes in the square waveguide. Therefore, the electric field distribution over the aperture of conventional MDH is identical in E- and H-planes, resulting in circularly symmetric field distribution. Additionally, focussing of microwave energy at the small spherical (or near spherical) tumor location is easily possible through symmetrical high resolution exposure. Hence, the conventional MDH designed at 2450/915 MHz and terminated in a phantom bio-

medium/bio-media may be one of the promising candidates for the treatment of localized near spherical or irregular-shaped tumors in superficial abdominal/thoracic region of the body.

In this chapter, direct-contact water-loaded conventional MDHs as hyperthermia applicators are investigated through simulation, theoretically and experimentally at 2450 MHz and through simulation and theoretically at 915 MHz. The proposed horns are assumed to be directly terminated in bio-medium/bio-media. Water-loading [Uzunoglu (1987), Nikita and Uzunoglu (1989)] of the MDH reduces any mismatch at the interface between the horn and bio-medium/bio-media since the effective dielectric permittivity of the bio-medium/bio-media is close to that of water. Hence, strong coupling between the antenna and bio-medium/bio-media takes place. Additionally, high value of the real part of relative permittivity of water ($\varepsilon'_w$=78) permits a considerable reduction (by a factor of $\cong$9) of the aperture size of conventional MDH, due to which size of the antenna reduces considerably. Moreover, leakage is minimum for a direct contact applicator [Kantor (1978)]. Hence, these types of applicators are desirable as compared to spaced applicators for hyperthermia application.

## 2.2 Design and/or fabrication of water-loaded conventional metal diagonal horns (MDHs)

Direct-contact water-loaded conventional MDHs were designed at 2450 and 915 MHz using computer simulation technology microwave studio (CST MWS) 2011 software, which is based on finite integration numerical technique. Further, the horn designed at 2450 MHz was fabricated to demonstrate the technical feasibility of the horn.

Geometry of water-loaded conventional MDHs for operation at ISM frequencies of 2450 and 915 MHz is shown in Figure 2.1. These horns were designed following the procedure given by Love [Love (1976)]. The horn designed at 2450 MHz was then fabricated using copper sheet of thickness = 2 mm. The design of each conventional MDH is concerned with proper selection of the different dimensions of the horn to get minimum reflection coefficient at the operating frequency. Filling a waveguide by a dielectric with relative dielectric

constant of $\varepsilon_r$, reduces the size of the antenna by a factor of $\sqrt{\varepsilon_r}$. The complex permittivity of water has been taken to be 77−j12.09 and 78−j3.09 [Gupta and Singh (2006)] at 2450 and 915 MHz respectively. Water-loaded horn antennas for operation at 2450 and 915 MHz have been assumed excited with higher frequency water-filled metal rectangular waveguides WR-34 and WR-112 respectively.

The aperture dimension (*d*) of the water-loaded conventional MDH to be designed at an ISM frequency is selected for required gain G, which can be found from the following relation [Love (1976)]:

$$G = 10 log \frac{4\pi\eta d^2}{\lambda_w^2} \tag{2.1}$$

where η is the efficiency of the horn, which can be taken equal to 0.81 [Love (1976)], and $\lambda_w (= \lambda / \sqrt{\varepsilon'_{rw}})$ is the effective wavelength at the design frequency of the horn, and $\varepsilon'_{rw}$ is the real part of the relative permittivity of water. Each conventional MDH was designed for 15 dB gain. The values of aperture dimension *'d'* of the horn antennas for ISM frequencies of 2450 and 915 MHz computed using equation (2.1) are given in Table 2.1. The throat dimension '$d_1$' of each horn is selected in such a way that $TE_{10}$ and $TE_{01}$ modes propagate inside the respective square cross-section waveguide at the throat. Propagation of other higher order modes is not allowed. To eliminate the higher order modes, the throat dimension '$d_1$' must be slightly greater than one-half wavelength, but less than three-half wavelengths [Love (1976)]. The transformer lengths '$T_1$' and '$T_2$' of the rectangular-to-circular, and circular-to-square waveguide transitions in each case are selected on the basis of quarter wave transformer concept to get minimum reflection coefficient at the design frequency. The diameter '*D*' of the circular waveguide at the design frequency is selected so that cut off wavelength of rectangular waveguide carrying $TE_{10}$ mode is equal to that of circular waveguide carrying $TE_{11}$ mode. All the waveguide sections discussed earlier and the horns are assumed to be completely filled with water. The dimension optimization of each proposed horn was carried out using CST MWS software.

The aperture of each conventional MDH is assumed to be surrounded by a conducting ground plane of copper in xy-plane so that the fringing electric field

outside the aperture becomes zero and backlobe disappear. The dimensions of the conducting ground plane are 150 mm × 150 mm × 2 mm and 250 mm × 250 mm × 2 mm for the conventional MDH antennas designed at 2450 MHz and 915 MHz respectively. $TE_{10}$ mode propagates in each input rectangular waveguide at the operating frequency. The input end of rectangular waveguide section of each horn antenna is short circuited. Each conventional MDH antenna is assumed to be excited with the help of coaxial probe inserted through a small hole cut in the middle of the broad wall of rectangular waveguide section at a distance of $\lambda_{g\varepsilon}/4$ from the short-circuited end, where $\lambda_{g\varepsilon}$ is the guide wavelength in water-loaded input rectangular waveguide for $TE_{10}$ mode given by the relation

$$\lambda_{g\varepsilon} = \frac{\lambda_w}{\sqrt{1-\left(\frac{f_{c_{10}}}{f}\right)^2}} \tag{2.2}$$

where $\lambda_w (= \lambda/\sqrt{\varepsilon'_{rw}})$ is already defined, $f_{c_{10}} = c/2a\sqrt{\varepsilon'_{rw}}$ is the cut off frequency for $TE_{10}$ mode, $c$ is the velocity of microwave in free space = $3 \times 10^8$ m/s, $a$ is the broad dimension of the input rectangular waveguide and $f$ is the design frequency.

The optimized dimensions of the horn antennas designed at 915 and 2450 MHz are given in Table 2.1.

**Table 2.1:** Design parameters of the water-loaded conventional MDH antennas

| Parameter | Symbol | Dimension (mm) | |
|---|---|---|---|
| | | 2450 MHz | 915 MHz |
| Length of input waveguide | $L_1$ | 12 | 20 |
| Transition length of circular waveguide | $T_1$ | 10 | 10 |
| Length of circular waveguide | $L_2$ | 2 | 2 |
| Diameter of circular waveguide | D | 10 | 33.4 |
| Transition length of square waveguide | $T_2$ | 13 | 12 |
| Length of square waveguide | $L_3$ | 4 | 3 |
| Throat size | $d_1$ | 9.1 | 29 |
| Length of flaring section | L | 46 | 110 |
| Aperture size | d | 24.6 | 65 |

Figure 2.2 shows different views of the fabricated horn for operation at 2450 MHz. SMA (Sub Miniature version A) connector was used for excitation of the water-loaded conventional MDH through coaxial probe.

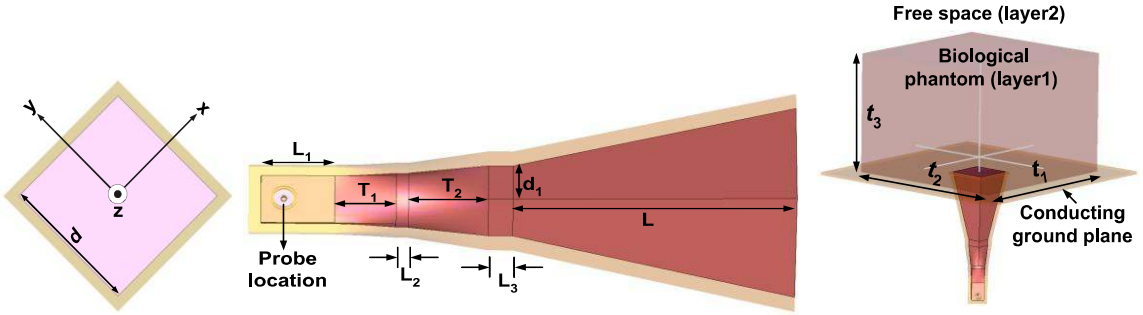


(a) (b) (c)

**Figure 2.1**: Geometry of conventional MDHs (a) top view, (b) side view, (c) terminated in a biological phantom.

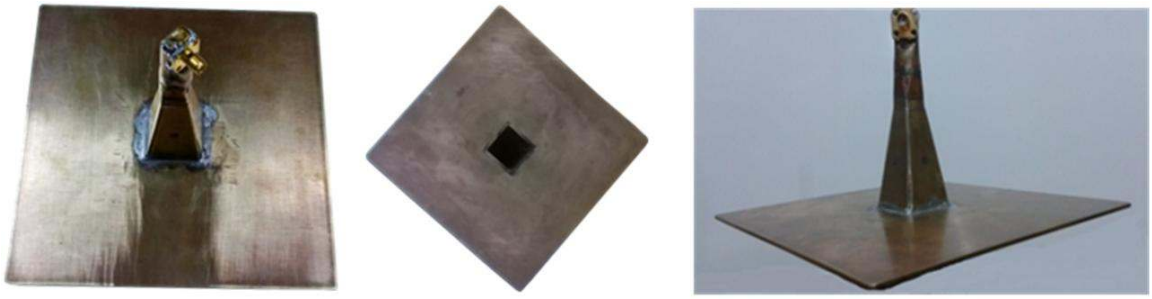

**Figure 2.2**: Different views of fabricated prototype for operation at 2450 MHz.

## 2.3 Water-loaded conventional MDH terminated in phantom muscle

Water-loaded conventional MDHs in direct contact with phantom muscle medium were designed at 2450 and 915 MHz using CST MWS 2011 software. The experimental study of SAR distributions in the phantom bio-medium of known physical properties [Stuchly and Stuchly (1980)] was carried out at 2450 MHz with the help of 50 Ω coaxial L-shaped and straight monopole probes and Agilent make spectrum analyser (Model E4448 A). The simulated results for SAR distribution in the phantom bio-medium at 2450 MHz are compared with the corresponding theoretical and experimental results and the simulation results for SAR distribution at 915 MHz are compared with the corresponding theoretical results. The theoretical investigation of fields in the planar phantom muscle medium due to each water-loaded conventional MDH antenna makes use of plane wave spectral technique for computation of SAR distribution in the medium. The theoretical field components and SAR distributions were numerically evaluated using MATLAB software.

### 2.3.1 *Analysis of electric field and specific absorption rate (SAR) in phantom muscle in direct contact with water-loaded conventional MDH*

In order to quantify the induced electric field in a biological phantom (muscle) due to the known field distribution at the aperture of a water-loaded conventional MDH terminated in the bi-layered media consisting of muscle and free space layers, theoretical analysis is presented. In the present analysis, the muscle layer is considered to be of finite thickness '$t_3$' followed by infinite free space layer. Muscle phantom and free space layers have relative permittivities of $\varepsilon_1^*$ and $\varepsilon_2$ respectively. The values of complex relative permittivity of the biological phantom are 50.00−j16.00 [Stuchly and Stuchly (1980)] and 55.00−j19.00 [Gabriel (1996)] at 2450 and 915 MHz respectively. The analysis of fields in bi-layered media presented here follows the plane wave spectral technique discussed by Compton [Compton (1964)] and Harrington [Harrington (1961)].

Previously, plane wave spectral technique was used to estimate the induced field components in the biological phantom due to the box-horn [Gupta and Singh (2006)] for which aperture field varies along one direction only, while the field remains constant along the transverse direction as given in references [Gupta and Singh (2006), Compton (1964), Harrington (1961)]. However, in case of the conventional MDH antennas, aperture field varies in both x- and y-directions due to the propagation of $TE_{10}$ and $TE_{01}$ orthogonal modes. The aperture of each conventional MDH antenna is assumed to be surrounded by infinite conducting ground plane in xy-plane. Each conventional MDH is a multimode horn antenna in which $TE_{10}$ and $TE_{01}$ modes are present at the aperture. In the present theoretical analysis, it is assumed that only $TE_{10}$ and $TE_{01}$ mode fields are present at the aperture and also aperture phase error is zero.

The x- and y-components of electric field at the aperture of a water-loaded conventional MDH antenna [Love (1976)] is represented by

$$E_{x_1}(\mathrm{x},\mathrm{y},0) = \mathrm{a}_{10}(1+\Gamma)\cos\left(\frac{\pi y}{d}\right) \tag{2.3}$$

$$E_{y_1}(\mathrm{x},\mathrm{y},0) = \mathrm{a}_{01}(1+\Gamma)\cos\left(\frac{\pi x}{d}\right) \tag{2.4}$$

where $a_{10}$ and $a_{01}$ are amplitude coefficients [Appendix-A] for $TE_{10}$ and $TE_{01}$ modes respectively and $\Gamma$ is reflection coefficient [Appendix-B] at the interface between water-loaded conventional MDH antenna and biological phantom (muscle) for each of these modes.

When the aperture electric field is given by equations (2.3) and (2.4), the fields in the bi-layered media (muscle and free-space layers) correspond to TE to *x* and TE to *y* modes [Compton (1964)]. Through the use of 'plane wave spectral technique' as given in references [Compton (1964), Harrington (1961)], spectral integral representations of the fields in the different layers are obtained.

The x-, y-, and z-components of electric fields in the muscle layer (layer1) and free space layer (layer2) are obtained as given in the reference [Gupta and Singh (2006)] are reproduced below.

$$E_{x1}(\mathrm{x},\mathrm{y},\mathrm{z}) = \frac{1}{2\pi^2}\int_{-\infty}^{\infty}\int_{-\infty}^{\infty}\left[-jk_{z1}I_{\psi_1}e^{-jk_{z1}z} + jk_{z1}R_{\psi_1}e^{jk_{z1}z}\right]e^{-jk_x x}e^{-jk_y y}dk_x dk_y \tag{2.5}$$

$$E_{y1}(\mathrm{x},\mathrm{y},\mathrm{z}) = \frac{1}{2\pi^2}\int_{-\infty}^{\infty}\int_{-\infty}^{\infty}\left[jk_{z1}I_{\phi_1}e^{-jk_{z1}z} - jk_{z1}R_{\phi_1}e^{jk_{z1}z}\right]e^{-jk_x x}e^{-jk_y y}dk_x dk_y \tag{2.6}$$

$$\begin{aligned}\mathrm{E}_{z1}(\mathrm{x},\mathrm{y},\mathrm{z}) = {} & \frac{1}{2\pi^2}\int_{-\infty}^{\infty}\int_{-\infty}^{\infty}\left[I_{\phi_1}e^{-jk_{z1}z} + R_{\phi_1}e^{jk_{z1}z}\right]e^{-jk_x x}(-\mathrm{j}k_y)e^{-jk_y y}dk_x dk_y \\ & -\frac{1}{2\pi^2}\int_{-\infty}^{\infty}\int_{-\infty}^{\infty}\left[I_{\psi_1}e^{-jk_{z1}z} + R_{\psi_1}e^{jk_{z1}z}\right](jk_x)e^{-jk_x x}e^{-jk_y y}dk_x dk_y\end{aligned} \tag{2.7}$$

$$E_{x2}(\mathrm{x},\mathrm{y},\mathrm{z}) = \frac{1}{2\pi^2}\int_{-\infty}^{\infty}\int_{-\infty}^{\infty} -jk_{z2}T_{\psi_1}e^{-jk_{z2}z}e^{-jk_x x}e^{-jk_y y}dk_x dk_y \tag{2.8}$$

$$E_{y2}(\mathrm{x},\mathrm{y},\mathrm{z}) = \frac{1}{2\pi^2}\int_{-\infty}^{\infty}\int_{-\infty}^{\infty} jk_{z2}T_{\phi_1}e^{-jk_{z2}z}e^{-jk_x x}e^{-jk_y y}dk_x dk_y \tag{2.9}$$

$$\begin{aligned}E_{z2}(\mathrm{x},\mathrm{y},\mathrm{z}) = {} & \frac{1}{2\pi^2}\int_{-\infty}^{\infty}\int_{-\infty}^{\infty}T_{\phi_1}e^{-jk_{z2}z}e^{-jk_x x}(-\mathrm{j}k_y)e^{-jk_y y}dk_x dk_y \\ & -\frac{1}{2\pi^2}\int_{-\infty}^{\infty}\int_{-\infty}^{\infty}T_{\psi_1}e^{-jk_{z2}z}(-\mathrm{j}k_x)e^{-jk_x x}e^{-jk_y y}dk_x dk_y\end{aligned} \tag{2.10}$$

where $I_{\psi_1}, I_{\phi_1}, R_{\psi_1}, R_{\phi_1}$ are plane wave spectra in muscle layer (layer 1), and $T_{\psi_1}$ and $T_{\phi_1}$ are plane wave spectra in free space layer (layer 2); $k_{z1}$ is the propagation constant in muscle layer along z-direction, and $k_{z2}$ is the propagation constant in free-space layer along z-direction; $k_x$ and $k_y$ are respectively the propagation constants along x-and y-directions.

Similarly, the x-, and y-components of magnetic field in the two layers (muscle and free-space layers) are derived

$$H_{x1}(\mathrm{x,y,z}) = \frac{1}{2\pi^2}\int_{-\infty}^{\infty}\int_{-\infty}^{\infty}\left\{\begin{array}{l}\dfrac{{k_1}^2-{k_x}^2}{j\omega\mu_0}\left[I_{\phi_1}e^{-jk_{z1}z}+R_{\phi_1}e^{jk_{z1}z}\right]\\ -\dfrac{k_xk_y}{j\omega\mu_0}\left[I_{\psi_1}e^{-jk_{z1}z}+R_{\psi_1}e^{jk_{z1}z}\right]\end{array}\right\}e^{-jk_xx}e^{-jk_yy}dk_xdk_y \tag{2.11}$$

$$H_{y1}(\mathrm{x,y,z}) = \frac{1}{2\pi^2}\int_{-\infty}^{\infty}\int_{-\infty}^{\infty}\left\{\begin{array}{l}\dfrac{{k_1}^2-{k_y}^2}{j\omega\mu_0}\left[I_{\psi_1}e^{-jk_{z1}z}+R_{\psi_1}e^{jk_{z1}z}\right]\\ -\dfrac{k_xk_y}{j\omega\mu_0}\left[I_{\phi_1}e^{-jk_{z1}z}+R_{\phi_1}e^{jk_{z1}z}\right]\end{array}\right\}e^{-jk_xx}e^{-jk_yy}dk_xdk_y \tag{2.12}$$

$$H_{z1}(\mathrm{x,y,z}) = \frac{1}{2\pi^2}\int_{-\infty}^{\infty}\int_{-\infty}^{\infty}\left\{\begin{array}{l}\dfrac{k_{z1}k_x}{j\omega\mu_0}\left[-I_{\phi_1}e^{-jk_{z1}z}+R_{\phi_1}e^{jk_{z1}z}\right]\\ -\dfrac{k_{z1}k_y}{j\omega\mu_0}\left[-I_{\psi_1}e^{-jk_{z1}z}+R_{\psi_1}e^{jk_{z1}z}\right]\end{array}\right\}e^{-jk_xx}e^{-jk_yy}dk_xdk_y \tag{2.13}$$

$$H_{x2}(\mathrm{x,y,z}) = \frac{1}{2\pi^2}\int_{-\infty}^{\infty}\int_{-\infty}^{\infty}\left\{\frac{{k_2}^2-{k_x}^2}{j\omega\mu_0}T_{\phi_1}-\frac{k_xk_y}{j\omega\mu_0}T_{\psi_1}\right\}e^{-jk_{z2}z}e^{-jk_xx}e^{-jk_yy}dk_xdk_y \tag{2.14}$$

$$H_{y2}(\mathrm{x,y,z}) = \frac{1}{2\pi^2}\int_{-\infty}^{\infty}\int_{-\infty}^{\infty}\left\{\frac{{k_2}^2-{k_y}^2}{j\omega\mu_0}T_{\psi_1}-\frac{k_xk_y}{j\omega\mu_0}T_{\phi_1}\right\}e^{-jk_{z2}z}e^{-jk_xx}e^{-jk_yy}dk_xdk_y \tag{2.15}$$

$$H_{z2}(\mathrm{x,y,z}) = \frac{1}{2\pi^2}\int_{-\infty}^{\infty}\int_{-\infty}^{\infty}\left\{\frac{-k_xk_{z2}}{j\omega\mu_0}T_{\phi_1}-\frac{k_yk_{z2}}{j\omega\mu_0}T_{\psi_1}\right\}e^{-jk_{z2}z}e^{-jk_xx}e^{-jk_yy}dk_xdk_y \tag{2.16}$$

where $k_1(=\omega\sqrt{\mu_0\varepsilon_0\mu_1^*\varepsilon_1^*})$ and $k_2(=\omega\sqrt{\mu_0\varepsilon_0\mu_2^*\varepsilon_2})$ is the propagation constant in muscle layer and free space layer. $\omega$ is the angular operating frequency. $\mu_0$ and $\varepsilon_0$ are the permeability and permittivity of free-space respectively.

By taking the inverse Fourier transform of equation (2.5) and (2.6) at z = 0, we get

$$jk_{z1}[-\mathrm{I}_{\psi 1}+\mathrm{R}_{\psi 1}]=f \tag{2.17}$$

where

$$f = \int_{-d/2}^{d/2}\int_{-d/2}^{d/2} a_{10}(1+\Gamma)\cos\left(\frac{\pi y}{d}\right)e^{jk_x x}e^{jk_x y}dxdy = \frac{4\pi d a_{10}(1+\Gamma)}{k_x(\pi^2 - k_y{}^2 d^2)}\sin\left(\frac{k_x d}{2}\right)\cos\left(\frac{k_y d}{2}\right)$$

and $\quad jk_{z1}[I_{\phi 1} - R_{\phi 1}] = g \qquad (2.18)$

where, $g = \int_{-d/2}^{d/2}\int_{-d/2}^{d/2} a_{01}(1+\Gamma)\cos\left(\frac{\pi x}{d}\right)e^{jk_x x}e^{jk_x y}dxdy = \frac{4\pi d a_{01}(1+\Gamma)}{k_y(\pi^2 - k_x{}^2 d^2)}\sin\left(\frac{k_y d}{2}\right)\cos\left(\frac{k_x d}{2}\right)$

By applying the boundary conditions, *i.e.* the continuity of tangential electric and magnetic fields at 'z = $t_3$' (the interface between muscle and free-space), remaining four equations are determined as follows:

$$-jk_{z1}I_{\psi_1}e^{-jk_{z1}t_3} + jk_{z1}R_{\psi_1}e^{jk_{z1}t_3} = -jk_{z2}T_{\psi_1}e^{-jk_{z2}t_3} \qquad (2.19)$$

$$jk_{z1}I_{\phi_1}e^{-jk_{z1}t_3} - jk_{z1}R_{\phi_1}e^{jk_{z1}t_3} = jk_{z2}T_{\phi_1}e^{-jk_{z2}t_3} \qquad (2.20)$$

$$\begin{aligned}&\left(k_1{}^2 - k_x{}^2\right)\left[I_{\phi_1}e^{-jk_{z1}t_3} + R_{\phi_1}e^{jk_{z1}t_3}\right] - k_x k_y\left[I_{\psi_1}e^{-jk_{z1}t_3} + R_{\psi_1}e^{jk_{z1}t_3}\right]\\ &= \left(k_2{}^2 - k_x{}^2\right)T_{\phi_1}e^{-jk_{z2}t_3} - k_x k_y T_{\psi_1}e^{-jk_{z2}t_3}\end{aligned} \qquad (2.21)$$

$$\begin{aligned}&\left(k_1{}^2 - k_y{}^2\right)\left[I_{\psi_1}e^{-jk_{z1}t_3} + R_{\psi_1}e^{jk_{z1}t_3}\right] - k_x k_y\left[I_{\phi_1}e^{-jk_{z1}t_3} + R_{\phi_1}e^{jk_{z1}t_3}\right]\\ &= \left(k_2{}^2 - k_y{}^2\right)T_{\psi_1}e^{-jk_{z2}t_3} - k_x k_y T_{\phi_1}e^{-jk_{z2}t_3}\end{aligned} \qquad (2.22)$$

The expressions for $R_{\psi 1}$ and $R_{\phi 1}$ obtained from equations (2.17) and (2.18) are substituted into equations (2.19) – (2.22) to obtain the following equations:

$$A_{11}I_{\phi 1} + A_{12}I_{\psi 1} = B_{11} \qquad (2.23)$$

$$A_{21}I_{\phi 1} + A_{22}I_{\psi 1} = B_{22} \qquad (2.24)$$

$$A_{11} = \left(k_1{}^2 - k_x{}^2\right)k_{z2}\cos k_{z1}t_3 + j\left(k_2{}^2 - k_x{}^2\right)k_{z1}\sin k_{z1}t_3 \qquad (2.25)$$

$$A_{12} = A_{21} = -k_x k_y(k_{z2}\cos k_{z1}t_3 + jk_{z1}\sin k_{z1}t_3) \qquad (2.26)$$

$$A_{22} = \left(k_1{}^2 - k_y{}^2\right)k_{z2}\cos k_{z1}t_3 + j\left(k_2{}^2 - k_y{}^2\right)k_{z1}\sin k_{z1}t_3 \qquad (2.27)$$

$$B_{11} = \frac{-j}{2}\left\{g\frac{k_{z2}}{k_{z1}}e^{jk_{z1}t_3}\left(k_1{}^2 - k_x{}^2\right) + k_x k_y f e^{jk_{z1}t_3} + f k_x k_y\frac{k_{z2}}{k_{z1}}e^{jk_{z1}t_3} + g e^{jk_{z2}t_3}\left(k_2{}^2 - k_x{}^2\right)\right\} \qquad (2.28)$$

$$B_{22} = \frac{j}{2}\left\{f\frac{k_{z2}}{k_{z1}}e^{jk_{z1}t_3}\left(k_1{}^2 - k_y{}^2\right) + g k_x k_y\frac{k_{z2}}{k_{z1}}e^{jk_{z1}t_3} + g k_x k_y e^{jk_{z1}t_3} + f e^{jk_{z2}t_3}\left(k_2{}^2 - k_y{}^2\right)\right\} \qquad (2.29)$$

$$I_{\phi 1} = \frac{\begin{vmatrix} B_{11} & A_{12} \\ B_{22} & A_{22} \end{vmatrix}}{\begin{vmatrix} A_{11} & A_{12} \\ A_{21} & A_{22} \end{vmatrix}}, I_{\psi 1} = \frac{\begin{vmatrix} A_{11} & B_{11} \\ A_{21} & B_{22} \end{vmatrix}}{\begin{vmatrix} A_{11} & A_{12} \\ A_{21} & A_{22} \end{vmatrix}} \tag{2.30}$$

Once the solution for $I_{\phi 1}$ and $I_{\psi 1}$ are obtained by using equation (2.30), other plane wave spectra such as $R_{\psi 1}, R_{\phi 1}, T_{\psi 1}$ and $T_{\phi 1}$ can be determined using equations (2.19) – (2.22).

The x-, y- and z-components of electric field in the muscle layer can then be found by using equations (2.5 – 2.7). The resultant electric field intensity in the muscle phantom is given by

$$|E|^2 = |E_{x1}|^2 + |E_{y1}|^2 + |E_{z1}|^2 \tag{2.31}$$

The SAR in the phantom muscle can be evaluated by

$$SAR = \frac{\sigma |E|^2}{2\rho} \tag{2.32}$$

where $|E|$ is the magnitude of total induced electric field strength inside the biological phantom, and σ and $\rho$ are the conductivity and density of the biological phantom respectively.

### 2.3.2 *Experimental technique for measuring electric field components in phantom muscle in direct contact with a water-loaded conventional MDH designed at 2450 MHz*

For a given volume of the phantom bio-medium, SAR is proportional to the square of the magnitude of induced electric field strength inside the phantom bio-medium and it is given by the relation

$$SAR = \frac{\sigma |E|^2}{2\rho} \tag{2.33}$$

where $|E|$ is the magnitude of total induced electric field strength inside the phantom bio-medium, and σ and $\rho$ are the conductivity and density of the phantom bio-medium respectively.

The experimental relative SAR distribution in the phantom bio-medium was determined at 2450 MHz with the help of Agilent make spectrum analyser (E4448A) and two 50 Ω coaxial monopole probes (one straight probe and another

L-shaped probe). Equation 2.33 can be used to compute relative SAR value at the point in the phantom bio-medium if the power proportional to $|E|^2$ is measured in the given bio-medium. The laboratory grade distilled water was used to fill the conventional MDH for operation at 2450 MHz (Figure 2.2). The material composition of the planar phantom bio-medium is taken to be 30% Gelatin + 69% Water + 1% NaCl [Stuchly and Stuchly (1980)]. The complex permittivity of the artificial phantom bio-medium (muscle medium) given in reference [Stuchly and Stuchly (1980)] is 50−j16 at 2450 MHz. The experimental setup for measuring the desired power level inside the phantom bio-medium in a particular direction due to the conventional MDH is shown in Figure 2.3(a). The power proportional to square of the magnitude of x-/y-/z-component of induced electric field at a point inside the bio-medium due to the applicator was detected with the help of coaxial monopole probes and spectrum analyser by keeping the axis of the corresponding probe along particular x-/y-/z-direction (Figure 2.3).

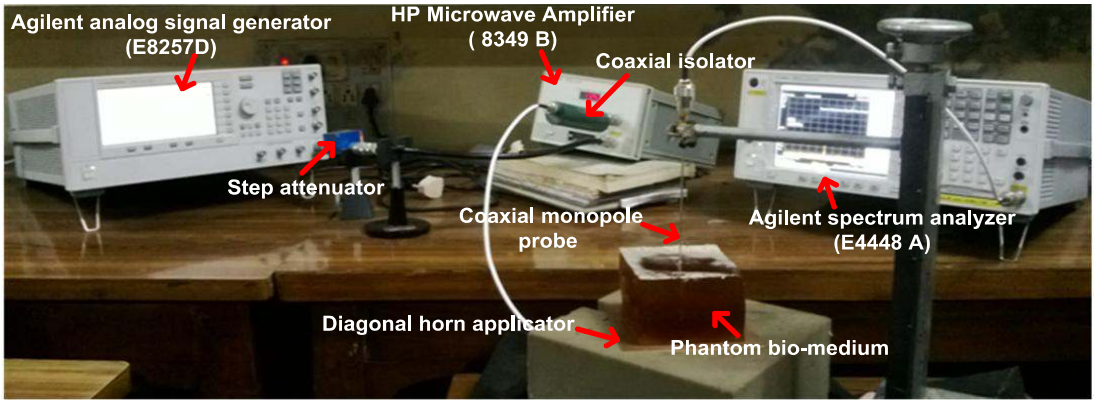


(a)

(b)

(c)

**Figure 2.3:** (a) Experimental setup for measurement of power level (proportional to square of the magnitude of induced electric field) in the phantom bio-medium, (b) coaxial straight monopole probe, and (c) coaxial L-shaped monopole probe.

Agilent make analog signal generator (E8257D) was connected to the fabricated water-loaded conventional MDH through Narda make step attenuator, HP (2-20 GHz, 20 dBm) microwave amplifier and Microlab make coaxial isolator as shown in Figure 2.3(a). A particular type of 50 Ω coaxial monopole probe was

connected to the RF in port of the spectrum analyser through a flexible coaxial cable (procured from M/S. Vidyut Yantra Udyog, Modinagar, U. P., India) as shown in Figure 2.3(b) and (c). The lengths of the extended inner conductors of straight and L-shaped coaxial probes are respectively equal to 14 and 12 mm. The power coupled from the analog signal generator and power amplifier combination to the phantom bio-medium through the water-loaded conventional MDH, which was designed and fabricated to operate at 2450 MHz, was sensed by a particular coaxial monopole probe. The spectrum analyser was configured to measure the power levels (in dBm) picked up by the probe, which was inserted inside the phantom bio-medium at 2450 MHz. The experimental determination of power level inside the phantom bio-medium which is proportional to square of the magnitude of x-/y-/z-component of induced electric field was carried out as detailed below. The power level corresponding to z-component of the induced field at a point in the phantom bio-medium which is proportional to $|E_z|^2$ was measured as a function of distance along x-/y-/z-direction by keeping the axis of the straight probe along z-direction and moving it along the desired x-/y-/z-direction while keeping remaining coordinates fixed. The power levels corresponding to x- and y-components of the induced electric field at a point inside the phantom bio-medium which are proportional to the $|E_x|^2$ and $|E_y{}^2|$ respectively were measured as a function of distance along x-/y-/z- direction by keeping the axis of the L-shaped probe along the x-/y-direction and moving it along the desired x-/y-/z-direction while keeping other coordinates fixed. The magnitude of the field component $|E_z{}^2|$ is small as compared to $|E_x|^2$ and $|E_y|^2$, however $|E_x|^2$ and $|E_y|^2$ are nearly same. The power proportional to square of the magnitude of each electric field component was sampled at a number of positions from 0 to ±56 mm along each of the x- and y-directions and from 0 to 80 mm along z-direction for water-loaded conventional MDH operating at 2450 MHz. The differing responses of 50 Ω L-shaped and straight coaxial probes in measuring the square of the magnitude of same field component were calibrated out through the application of correction factor. During measurement, coaxial

probes with plastic sheaths were used to prevent the probes getting short circuited when they are inserted into the phantom bio-medium for probing the fields.

The total induced electric field inside the phantom bio-medium at a particular point is given by

$$|E|^2 = |E_x|^2 + |E_y|^2 + |E_z|^2 \tag{2.34}$$

where, $E_x$, $E_y$ and $E_z$ are the induced electric field components along x-, y- and z-directions respectively.

The measured power levels at different points inside the phantom muscle medium were converted to experimental relative SAR distribution through the application of equations (2.33) and (2.34).

### 2.3.3 *Results and discussion*

#### 2.3.3.1 *Applicators' characteristics*

The simulated values of input reflection coefficient of the water-loaded conventional MDH antennas, each terminated in a phantom bio-medium are -17dB and -33 dB at 2450 and 915MHz respectively, which indicates good matching of the applicators to the feed at both operating frequencies.

The measured value of input reflection coefficient of the proposed antenna designed at 2450 MHz and terminated in the phantom bio-medium (muscle) is -12.9 dB.

Moreover, reflection coefficient at the interface of each conventional MDH applicator and the biological phantom has also been estimated theoretically as mentioned in sub-section 2.3.1 and Appendix-B. The estimated value of the said reflection coefficient for $TE_{10}$ (= $TE_{01}$) mode of the horn designed at 2450 MHz is -25 dB. Similarly, corresponding reflection coefficients values for the horn designed at 915 MHz is -27.8 dB. The values of reflection coefficient obtained at the interface of each conventional MDH antenna and muscle phantom indicates that reasonably good impedance matching between the horn aperture and the biological phantom is achieved at both the frequencies, though matching is better at 915 MHz.

#### 2.3.3.2 *Simulated SAR distributions in phantom muscle medium*

The applicator's design data along with dielectric properties of biological phantom discussed in sections 2.2 and 2.3, and given in Table 2.1 have been used in the estimation of simulated SAR distributions at the two operating frequencies of 2450 and 915 MHz. The density of biological phantom was chosen to be 1050 kg/m$^3$. The simulated normalized SAR distributions inside the biological phantom (muscle phantom) of size ($t_1 \times t_2 \times t_3$) = 200 mm × 200 mm × 150 mm (at 915 MHz) and 112 mm ×112 mm × 80 mm (at 2450 MHz) due to the respective water-loaded conventional MDH antennas were determined using CST MWS software and the results are shown in Figures 2.4 and 2.5. Initially, power fed to each antenna was assumed to be 1W in the simulation study.

#### 2.3.3.3 *Theoretical SAR distributions in phantom muscle medium*

The theoretical normalized SAR distributions in the muscle phantom were obtained by numerically solving the equations given in section 2.3 using MATLAB software and the results are given in Figures 2.4–2.6. In order to validate the circular symmetric behavior of SAR distributions in the biological phantom due to the conventional MDH antennas at 2450 and 915 MHz, normalized SAR distributions in xy-plane were obtained through theoretical analysis at z = 10 mm and the results are shown in Figure 2.6. These results clearly demonstrate the circular symmetry property of the SAR distributions in the transverse xy-plane in the muscle medium.

#### 2.3.3.4 *Experimental SAR distribution in phantom muscle medium at 2450 MHz*

The relative SAR distributions inside the phantom muscle measured with the help of coaxial monopole probes and spectrum analyser for the antenna operating at 2450 MHz are shown in Figures 2.4 and 2.5.

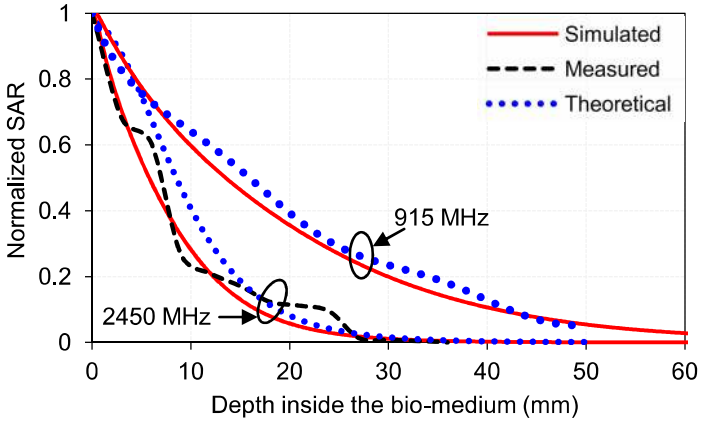


**Figure 2.4:** Normalized SAR distributions in phantom muscle in direct contact with water-loaded conventional MDHs at 2450 and 915 MHz along z-direction (x = y = 0).

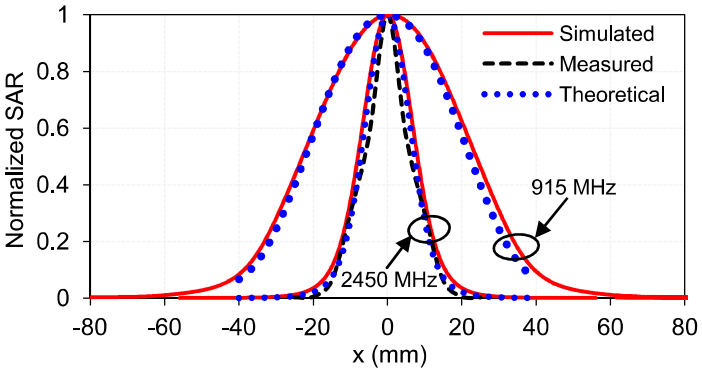


(a)

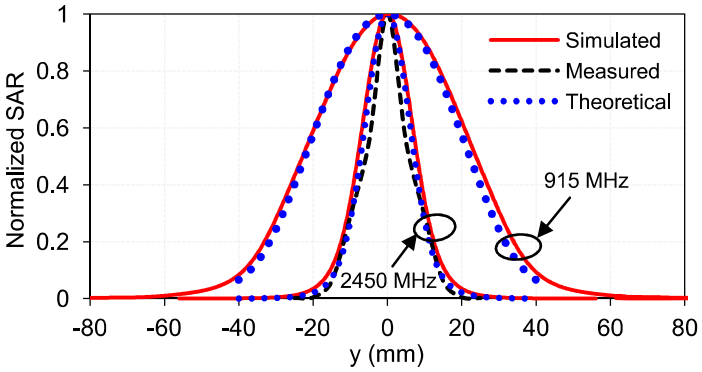


(b)

**Figure 2.5:** Normalized SAR distributions in phantom muscle in direct contact with water-loaded conventional MDHs at 2450 and 915 MHz along (a) x-direction at z = 10 mm (y = 0) and (b) y-direction at z = 10 mm (x = 0).

### 2.3.3.5 *Comparison of simulated, theoretical and/or experimental SAR distributions*

Figure 2.4 illustrates the normalized SAR distributions in the homogeneous biological phantom in z-direction due to the water-loaded conventional MDHs operating at 2450 and 915 MHz. Different curves of the relative SAR distributions were obtained by normalizing the absolute SAR values of the curves with

respective peak absolute SAR values (reference values). That is why, value of maximum normalized SAR value for all described curves is identical. The simulated, theoretical and/or experimental values of penetration depth (PD) in biological phantom (depth where SAR value is down to 13.5 percent of the maximum in the muscle) extracted from Figure 2.4 are given in Table 2.2 for conventional MDH antennas designed at 2450 and 915 MHz. It can be observed from Figure 2.4 and Table 2.2 that simulated values of PD is nearly in agreement with corresponding theoretical and/or experimental value(s) at each ISM frequency of interest. Further, simulated/theoretical/experimental PD in the bio-medium is higher for the antenna designed at lower ISM frequency.

The EFS is defined as the area that is enclosed within 50% SAR contour inside the biological phantom. Resolution of hyperthermia applicator in transverse directions is represented by EFS and for high transverse resolution, the value of EFS must be small. The simulated, theoretical and/or experimental values of EFS extracted from Figure 2.5 due to the water-loaded conventional MDHs are given in Table 2.2. It can be observed from Table 2.2 that simulated value of EFS is nearly in agreement with corresponding theoretical and/or experimental EFS value(s) at each frequency of interest. It can also be inferred from Table 2.2 that EFS in the bio-medium is higher for the antenna designed at lower ISM frequency. Further, simulated, theoretical and/or experimental values of EFS in the bio-medium exhibit circular symmetry at 2450 and 915 MHz. The diagonal horn, which is a multimode horn antenna supporting $TE_{10}$ and $TE_{01}$ modes has identical field distribution in E- and H-planes. That is why, circularly symmetric EFS is obtained due to the conventional MDHs at both the frequencies.

It can be seen from Figures 2.4 and 2.5 that the simulated, theoretical and/or experimental SAR distributions are nearly in agreement with each other at each ISM frequency of interest. Thus, the validity of plane wave spectral technique is proved through simulated/experimental SAR distributions. It can also be observed that theoretical results of SAR distributions are deviating to a smaller degree from the corresponding simulation and/or experimental results. The deviation in the results may be due to the factors given in the following. In theoretical analysis,

conducting ground plane surrounding the conventional MDH aperture extends upto infinity while finite size of the conducting ground plane has been taken in simulation studies. The effect of generation of higher order modes near the discontinuity regions including the aperture of the conventional MDH is not considered in the theoretical analysis. The accuracy of the experimental results could be affected by the accuracy with which the position of the particular monopole probe is measured. For the present case accuracy of position measurement is ±0.2 cm. The finite size of the coaxial probe inserted inside the bio-medium may distort the induced electric field to some extent. Although these factors individually may not cause much effect on the SAR value, but when taken collectively, they may become significant cause of deviation between the theoretical, simulated and/or experimental SAR values.

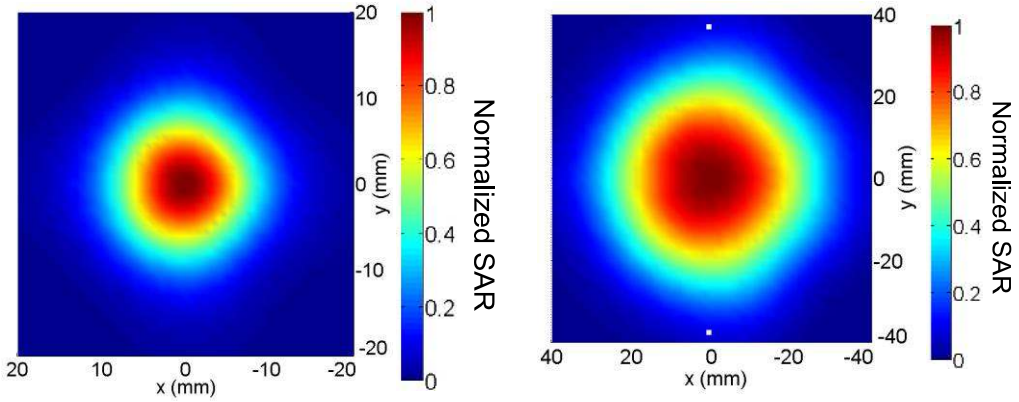


(a) (b)

**Figure 2.6:** Theoretical normalized SAR distribution inside the biological phantom in xy-plane at z = 10 mm due to water-loaded conventional MDH antenna designed at (a) 2450 MHz and (b) 915 MHz.

**Table 2.2:** SAR parameters in the biological phantom due to the conventional MDH antennas designed at 2450 and 915 MHz

| SAR parameters | | Frequency (MHz) | |
|---|---|---|---|
| | | 2450 | 915 |
| PD (mm) | Simulated | 15 | 36 |
| | Measured | 17 | – |
| | Theoretical | 16.8 | 39 |
| EFS ($mm^2$) | Simulated | 16 × 16 | 46 × 46 |
| | Measured | 13 × 13 | – |
| | Theoretical | 15 × 15 | 44 × 44 |

## 2.4 Simulation study on water-loaded conventional MDH terminated in tri-layered bio-media without and with tumor

The work presented in preceding sections is extended by performing simulation study on two water-loaded conventional MDHs (designed at 2450 and 915 MHz), each in direct contact with tri-layered bio-media (skin, fat and muscle layers) without and with embedded tumor for determination of SAR and/or temperature distributions using CST MWS software. The performance of each water-loaded MDH applicator is now studied through simulation for three tri-layered bio-models (one without tumor, and the other two consisting of superficial oval- and irregular-shaped abdominal/limb tumors) lying inside the muscle tissue taken one at a time as shown in Figure 2.7. The locations of oval- and irregular-shaped tumors embedded within second and third tri-layered bio-models considered for each of the applicators designed at 2450 and 915 MHz are provided in Figure 2.8. In all, four tumors of different shapes/sizes (two for each of the applicators) were considered in the present study. For heating of tumors designated as tumor1 (oval-shaped) and tumor2 (irregular-shaped), water-loaded conventional MDH designed at 2450 MHz which is in direct contact with tri-layered bio-media containing these tumors (one at a time) was considered. For the treatment of tumors designated as tumor3 and tumor4, water-loaded conventional MDH designed at 915 MHz which in direct contact with tri-layered bio-media containing the aforesaid tumors (one at a time) was considered. A cancerous tissue is known to have higher water content [Michaelson and Lin (1987)], and therefore higher dielectric constant and conductivity. The detailed dimensions and dielectric properties of tumors are mentioned in Figure 2.8/Table 2.3.

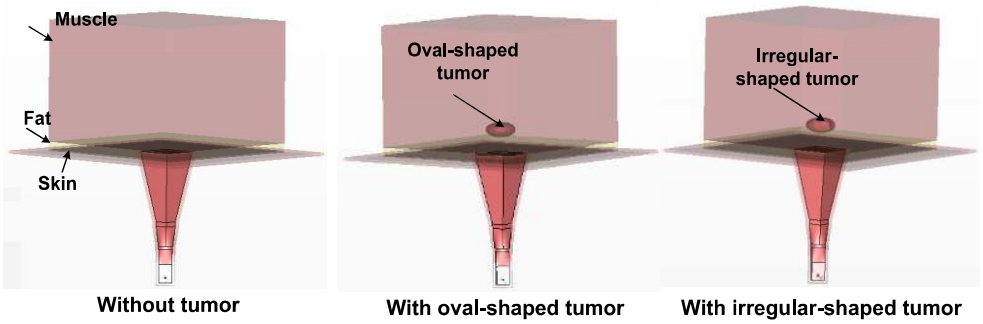


**Figure 2.7:** Conventional MDH antenna designed at a given frequency and terminated in tri-layered bio-media.

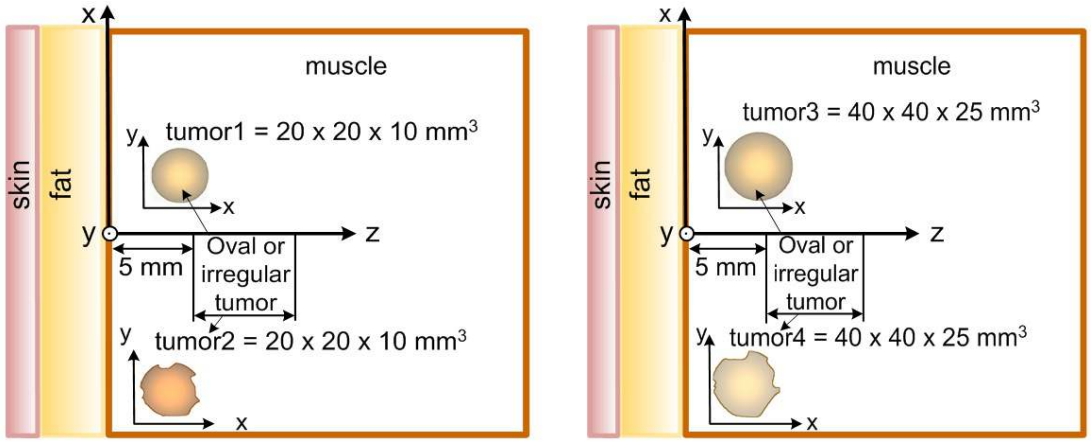


**Figure 2.8:** Two-dimensional realistic tri-layered bio-model with embedded (a) tumor1/tumor2 (applicable for the horn designed at 2450 MHz) and (b) tumor3/tumor4 (applicable for the horn designed at 915 MHz).

**Table 2.3:** Properties of bio-media and tumor [Stuchly and Stuchly (1980), Gabriel (1996)].

| Tissue/Tumor | Thickness (mm) | Density ($kg/m^3$) | $\varepsilon_r$ at 2450 MHz | $\varepsilon_r$ at 915 MHz |
|---|---|---|---|---|
| Skin | 1 | 1130 | 42-j12 | 46-j16.7 |
| Fat | 5 | 920 | 5.28-j0.76 | 11.3-j2.16 |
| Muscle | 80 | 1050 | 50-j16 | 55-j19 |
| Tumor1/Tumor2 | 10 | 1050 | 56-j21.3 | - |
| Tumor3/Tumor4 | 25 | 1050 | - | 58-j21.6 |

### 2.4.1 *SAR distributions without and with tumor*

Absolute value of peak SAR in the bio-model is dependent on input power, tissue composition and frequency for the given wave polarization and applicator-tissue separation. Figure 2.9 shows the simulated variations of peak SAR (inside muscle layer) with power fed to the water-loaded conventional MDHs designed at 2450 and 915 MHz which is in direct contact with a bio-model without tumor by taking the composition of bio-model as a parameter in each case and keeping the wave polarization unchanged. It can be observed from Figure 2.9 that as input power increases, peak SAR in the muscle layer increases for both bio-models. But for same input power, the value of peak SAR is smaller for tri-layered skin-fat-muscle model as compared with the homogeneous bio-model. This is due to the existence of reflections at various interfaces of the tri-layered bio-model. Further, keeping other parameters constant, peak SAR values increases with increase in

frequency. Increase in conductivity of the tissue with frequency plays significant role in increasing peak SAR value with frequency.

Simulations were also performed for normalized SAR distributions in tri-layered bio-media (skin, fat and muscle) without and with embedded tumors (taken one at a time) due to the water-loaded conventional MDHs (designed at 2450 and 915 MHz) to which 1 W input power was applied and the corresponding results are depicted in Figures 2.10-2.12.

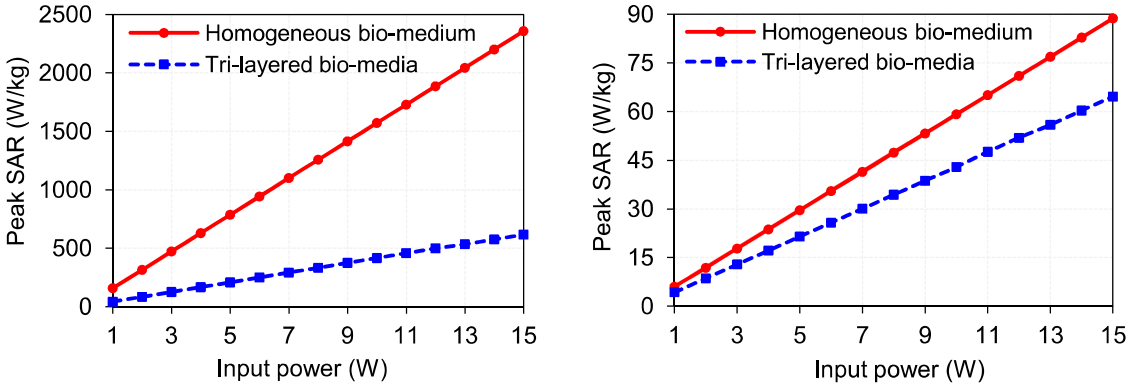


**Figure 2.9:** Variations of peak SAR with input power at (a) 2450 MHz and (b) 915 MHz.

Figure 2.10(a) and (b) show the simulated variations of normalized SAR distributions in the inhomogeneous tri-layered bio-media without and with embedded tumor1 and tumor2 (taken one at a time), along z-direction (for x=y=0) due to the water-loaded conventional MDHs designed respectively at 2450 and 915 MHz whereas Figures 2.11 and 2.12 show the variations of normalized SAR distributions in the said configurations of bio-media along x-/y-direction due to the aforesaid horns designed respectively at 2450 and 915 MHz. The values of PD and EFS for the frequencies of 2450 MHz and 915 MHz extracted from Figures 2.10–2.12 are given in Table 2.4. It can be seen from Table 2.4 that the values of PD and EFS are significantly higher at 915 MHz as compared to those at 2450 MHz. Further, the presence of a tumor does not alter PD and EFS (in the middle of tumor) significantly in each case. Additionally, it is observed that PD in the tri-layered bio-model due to the water-loaded conventional MDH designed at 2450 MHz is not sufficient to heat whole tumor depth effectively. Also, relative SAR

value observed at the skin surface using each of the proposed water-loaded conventional MDH applicators is maximum.

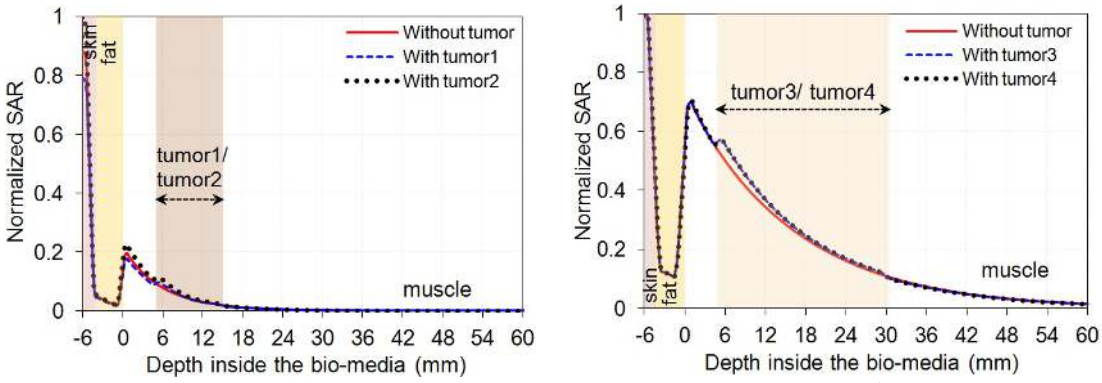


**Figure 2.10:** Simulated normalized SAR distributions inside the tri-layered bio-model without and with embedded tumors along z-direction (x = y = 0) due to the water-loaded conventional MDH for 1 W input power designed at (a) 2450, and (b) 915 MHz.

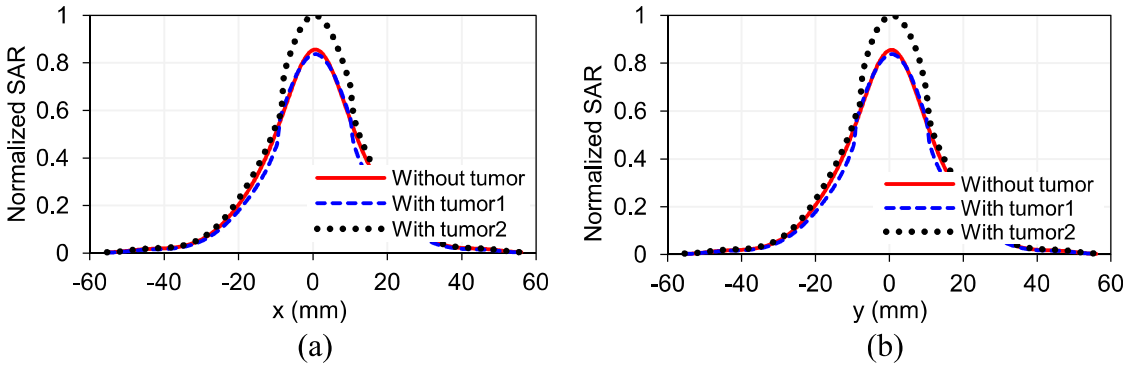


**Figure 2.11:** Simulated normalized SAR distributions inside the tri-layered bio-model without tumor, with embedded tumor1 and with embedded tumor2 due to the water-loaded conventional MDH at 2450 MHz along (a) x-direction at z = 10 mm (middle of tumor1/tumor2) (y = 0), and (b) y-direction at z = 10 mm (middle of tumor1/tumor2) (x = 0).

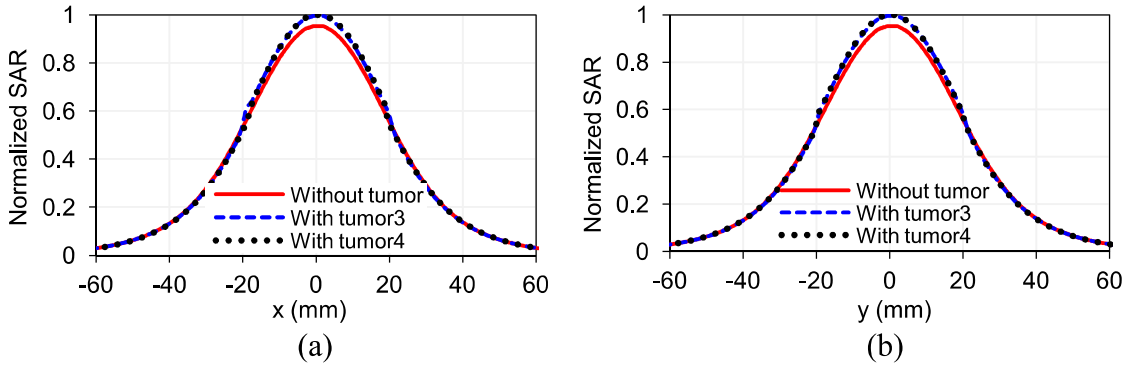


**Figure 2.12:** Simulated normalized SAR distributions inside the tri-layered bio-model without tumor, with embedded tumor3 and with embedded tumor4 due to the water-loaded conventional MDH designed at 915 MHz along (a) x-direction at z = 17.5 mm (middle of tumor3/tumor4) (y = 0), and (b) y-direction at z = 17.5 mm (middle of tumor3/tumor4) (x = 0).

### 2.4.2 *Temperature distributions without and with tumor*

The hyperthermia performance is characterized through the study of temperature distribution in a realistic tri-layered bio-model. The heat generated by the EM energy absorbed in the tissue is proportional to SAR. The bio-heat equation represents the relationship between the rate of EM energy absorbed into the tissue and the resulting rise in tissue temperature. The temperature distribution inside a realistic tri-layered bio-model can be evaluated by using Pennes' bio-heat equation (BHE) [Pennes (1948)] given below

$$\rho C \frac{\partial T}{\partial t} = \nabla \cdot (K \nabla T) + A_0 + \rho SAR - B(T - T_B) \tag{2.35}$$

where $\rho$ is the muscle density, $C$ is the specific heat of tissue, $K$ is the muscle thermal conductivity, $A_0$ is the metabolic heat production, $B$ is heat exchange mechanism due to capillary blood perfusion, $T_B$ is the blood temperature assumed to be constant (=$37^0$ C, the normal body temperature).

Since water-loaded conventional MDH designed at 2450 MHz is not able to heat effectively whole tumor embedded within the bio-medium/bio-media, its study as hyperthermia applicators to heat tumor embedded within realistic tri-layered bio-models is not extended further.

In order to characterize the hyperthermia treatment system, inhomogeneous tri-layered bio-models fed through water-loaded conventional MDH designed at 915 MHz was considered. CST multiphysics simulation software was used for thermal simulation at an initial temperature of $37^oC$ in which convective heat transfer coefficient between tissue and fluid of water-loaded applicator is assumed to be zero. The thermal parameters of bio-models used in simulation are listed in Table 2.5.

Figure 2.13 shows the variations of temperature as a function of depth in the tri-layered bio-model without tumor due to water-loaded conventional MDH designed at 915 MHz by taking input power level as a parameter. It can be seen from Figure 2.13 that as the power fed to the applicator increases, the temperature in the bio-media rises. As expected, the temperature decreases exponentially with depth inside the bio-media. It can also be inferred from Figure 2.13 that the

desired temperature range (41 – 45 $^{o}$C) for effective hyperthermia was achieved for input power level of 13 W for the water-loaded conventional MDH antenna designed at 915 MHz.

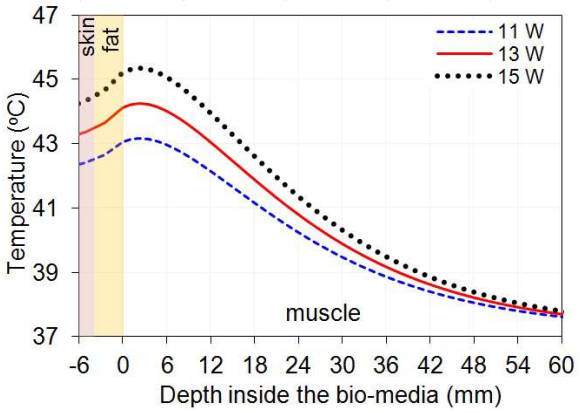


**Figure 2.13:** Temperature distribution inside the tri-layered bio-media without tumor for different input power levels along z-direction (x=y=0) due to water-loaded conventional MDH designed at 915 MHz.

Figures 2.14 shows the variations of temperature in the biological media with time due to the water-loaded conventional MDH designed at 915 MHz for normal bio-model without tumor and the model with embedded irregular tumor (tumor4) by taking depth in the tumor as a parameter. The power fed to the applicator for each bio-model was taken as 13 W. It is noticed that tumor temperature in each case reaches to a higher value as compared with normal tissue temperature [Figure 2.14 and Table 2.4]. This would aid in effective preferential heating of tumor in the superficial region of the body in comparison to normal tissue. Further, it can be observed from Figures 2.14 that initial rate of rise of temperature is higher at lower depth in the realistic tri-layered bio-media without/with embedded tumor4. The rate of rise of temperature in each case slows down after 30 minutes of heating and the tissue temperature approaches a steady value after about 50 minutes of heating at a given depth. The results demonstrate that tissue temperature approaches saturation after about 50 minutes of heating at a given depth and shows decreasing trend as depth increases.

Figures 2.15 shows the profiles of temperature along z-direction in the inhomogeneous tri-layered bio-media without and with embedded tumor (tumor3/tumor4) due to the water-loaded conventional MDH designed at 915

MHz for optimum input power of 13 W by taking tumor configuration as a parameter.

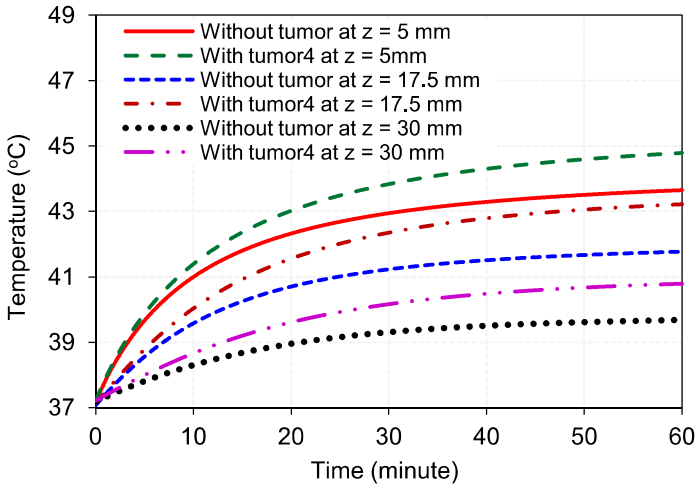


**Figure 2.14:** Variations of temperature in the realistic tri-layered bio-media without and with embedded tumor4 versus time due to the conventional MDH designed at 915 MHz by taking depth in the tumor as a parameter for x = y = 0.

It can be observed from Figure 2.15 that temperature profiles are similar for different tumor shapes. Moreover, the applicator designed at 915 MHz provides sufficient heating for the tumor embedded in the bio-model (Figure 2.15 and Table 2.4). Further, the depth at which temperature elevation is half of the maximum with respect to initial temperature (=ΔT/2) [derived from Figure 2.15 in each case] is given in Table 2.4. Further, it is observed that the presence of tumor of one configuration or another affects to certain degree the temperature distribution along the depth at the frequency of interest. Also, heating of skin surface is observed using applicator designed at ISM frequency of 915 MHz.

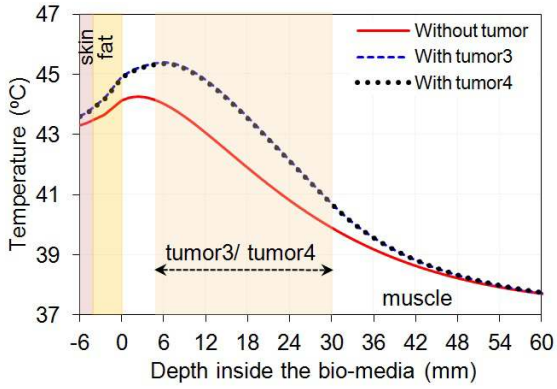


**Figure 2.15:** Simulated temperature distributions inside the tri-layered bio-models without and with embedded tumors along z-direction (x = y = 0) due to the conventional MDH for 13 W optimum input power at 915 MHz.

Figure 2.16(a), (b) and (c) depict the profiles of temperature distributions in the bio-models along x-/y-direction (y/x=0) for different depths without tumor, with embedded tumor3 and embedded tumor4 at different depths of tumor due to the water-loaded conventional MDH at 915 MHz for optimum input power of 13 W. The results show that water-loaded conventional MDH designed at 915 MHz is able to heat whole tumor volume effectively.

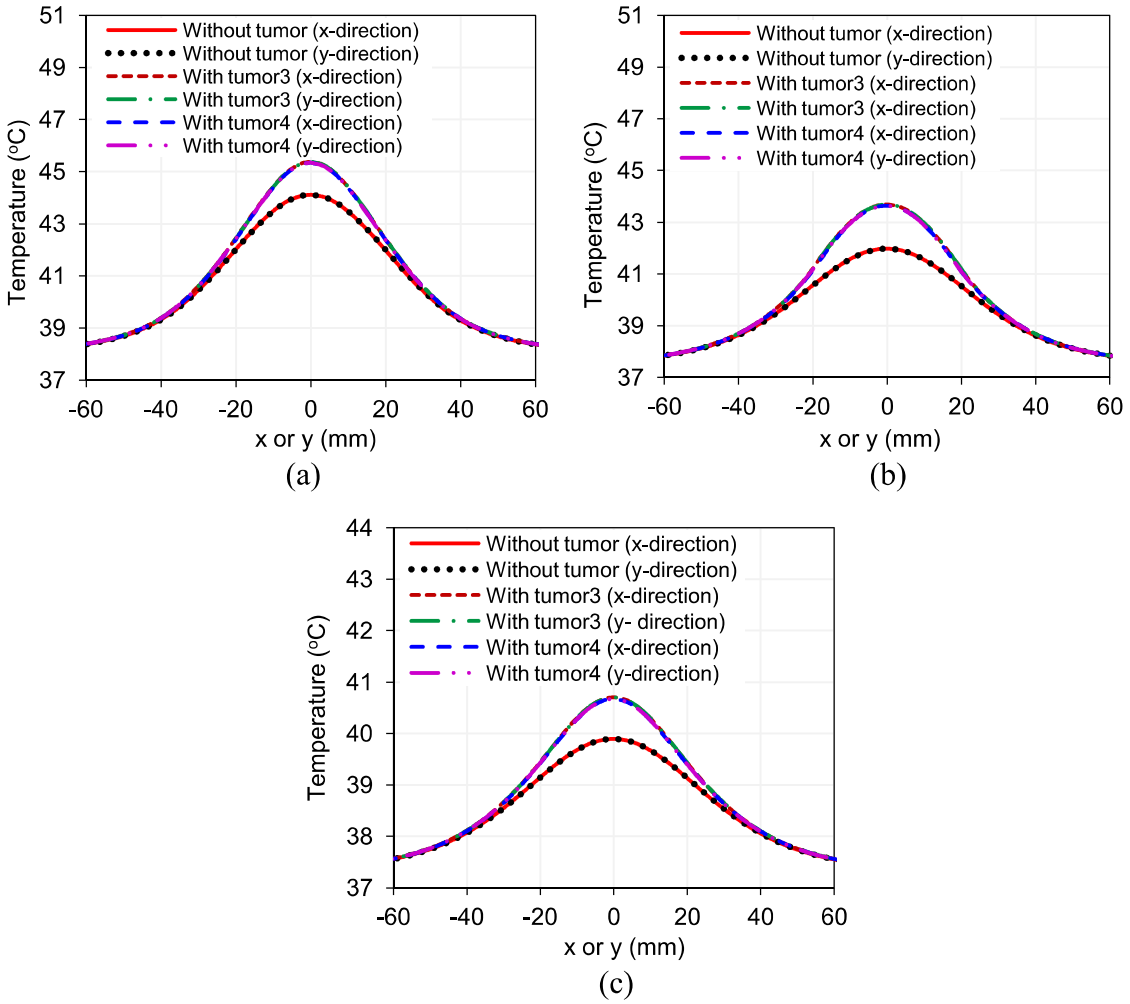


**Figure 2.16:** Simulated temperature distributions inside the tri-layered bio-model without tumor, with embedded tumor3 and with embedded tumor4 along x-/y-direction (y/x=0) at (b) z = 5 mm, (b) z = 17.5 mm, and (c) z = 30 mm due to the conventional MDH designed at 915 MHz for optimum input power of 13 W.

Figure 2.17(a), (b), (c) and (d) shows the cross-sectional profiles of temperature distribution in the bio-models without and with tumor3/tumor4 in xz-plane (for y =0), yz-plane (for x =0), with embedded tumor3 in xy-plane for z = 6 mm, 17.5 mm, and 29 mm, and with embedded tumor4 in xy-plane for z = 6 mm, 17.5 mm, 29 mm respectively owing to the water-loaded conventional MDH

designed at 915 MHz. It can be seen that desired temperature range (41– 45 $^{o}$C) is maintained in the whole volume of superficial tumors for effective hyperthermia. Symmetrical temperature distributions in the muscle medium due to the conventional MDH applicator can be observed in the transverse xy-plane [Figures 2.17 (c), (d)].

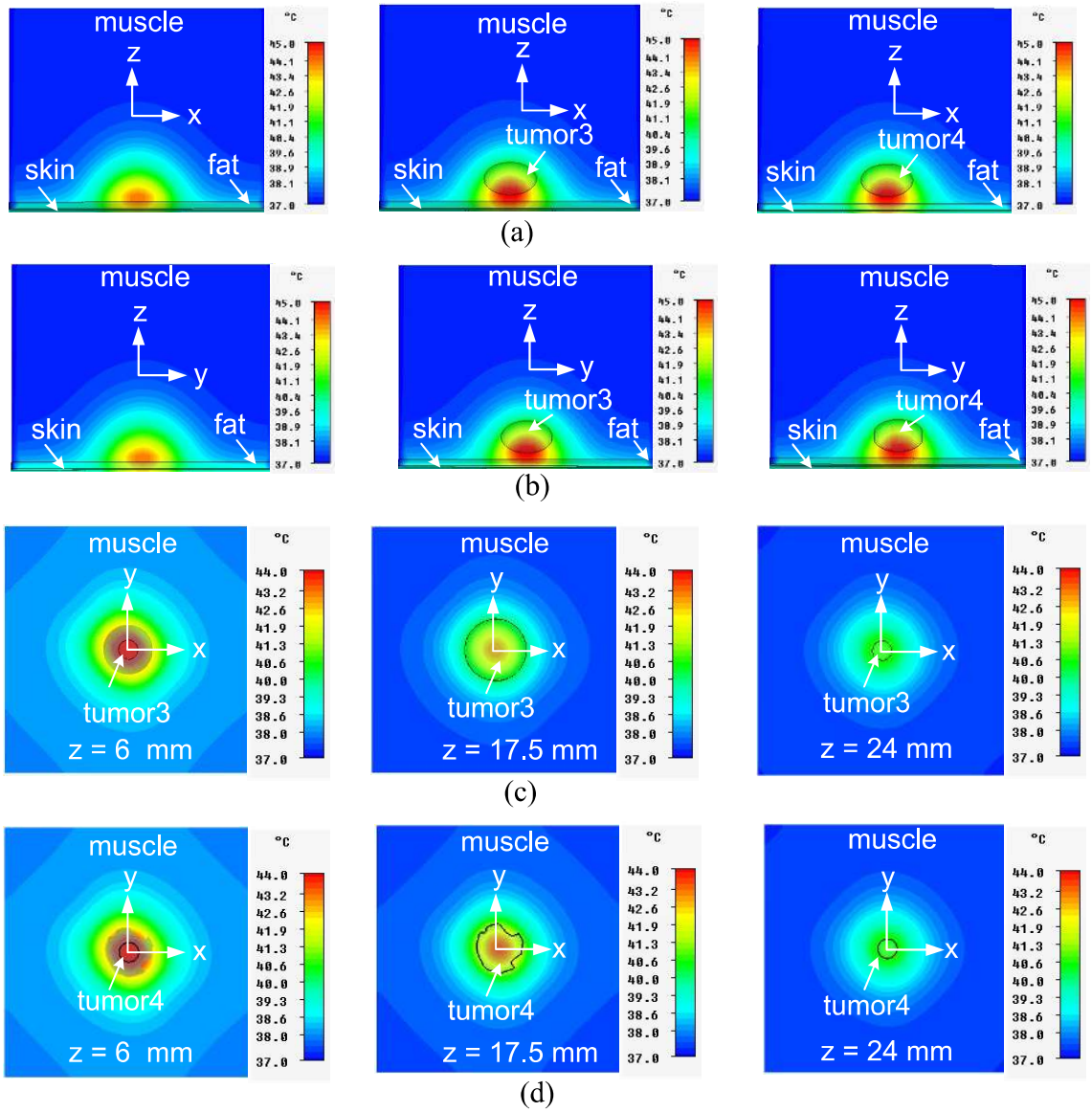


**Figure 2.17:** Simulated temperature distributions inside the realistic tri-layered bio-media without and with embedded tumor3/tumor4 due to the conventional MDH at 915 for 13 W optimum input power in (a) xz-plane, (b) yz-plane, (c) xy-plane with tumor3, and (d) xy-plane with tumor4.

**Table 2.4:** Hyperthermia performance due to the water-loaded conventional MDHs

| Freq. (MHz) | Inhomogeneous model | PD (mm) | EFS$^{\$}$ (mm$^2$) | Depth at ΔT/2 (mm) | Heating area$^{\$}$ {41-45$^o$C} (mm$^2$) |
|---|---|---|---|---|---|
| 2450 | Without tumor | 9.5 | 25.23 × 25.2 | - | - |
| | With tumor1 | 9.56 | 22.6 × 22.6 | - | - |
| | With tumor2 | 9.43 | 23.3×23.3 | - | - |
| 915 | Without tumor | 32.93 | 44.6 × 44.6 | 32 | 31.7 × 31.7 |
| | With tumor3 | 32.92 | 42.5 × 42.5 | 34 | 42.16 × 42.16 |
| | With tumor4 | 32.92 | 42.1 × 42.1 | 34 | 40.84 × 40.84 |

$^{\$}$EFS and heating area are defined in the middle of tumor.

**Table 2.5:** Thermal parameters of bio-media for the BHE [Gong and Wang (2009)]

| Tissue type | $\rho$ (kg/m$^3$) | $C$ (kJ/kg$^0$C) | $K$ (W/m$^0$C) | $A_0$ (W/m$^3$) | $B$ (W/m$^{3o}$C) |
|---|---|---|---|---|---|
| Skin | 0.42 | 3.5 | 0.42 | 1620 | 9100 |
| Fat | 920 | 2.5 | 0.25 | 300 | 1700 |
| Muscle | 1050 | 3.6 | 0.5 | 480 | 2700 |
| Tumor | 1050 | 3.6 | 0.5 | 480 | 675 |

## 2.5 Chapter summary

In the present chapter, water-loaded conventional metal diagonal horns (MDHs) have been investigated through simulation, theoretically and/or experimentally for hyperthermia application at 2450 and 915 MHz. The study involved determination of SAR and temperature distributions in a planar biological phantom/realistic tri-layered bio-media without and with embedded tumors due to the water-loaded conventional MDHs. The temperature distributions in the realistic bio-models obtained through thermal simulation indicate that the conventional MDH designed at 915 MHz with 13 W input power can be used as hyperthermia applicator for oval-/irregular-shaped tumors in superficial abdominal/thoracic region of the body.

Although diagonal horn provides circularly symmetric heating pattern but PD in the bio-media is not good enough to heat tumors at greater depth. Moreover, heating of skin surface in the tri-layered bio-model is also observed due to the water-loaded conventional MDHs. Therefore, it is advisable to modify the

aperture field distribution of the water-loaded conventional MDH without changing the aperture size at a given frequency in order to obtain enhanced PD in addition to symmetric EFS in the biological media.

In the next chapter, the investigation on water-loaded improved metal diagonal horns as hyperthermia applicators is presented to effectively heat appropriate size tumors at 2450 and 915 MHz. Each applicator under study is in direct contact with a bio-medium/realistic tri-layered bio-media without and with oval-/irregular-shaped tumors.